Supporting Information for

Controlling Interfacial Properties in Supported Metal Oxide Catalysts through Metal-Organic Framework Templating

Carter W. Abney,[†]* Jacob T. Patterson,[†‖] James C. Gilhula,[†¶] Li Wang,[†#] Dale K. Hensley,[‡] Jihua Chen,[‡] Guo Shiou Foo,[†] Zili Wu,[†] and Sheng Dai[†§]

† Chemical Sciences Division, Oak Ridge National Laboratory, Oak Ridge, TN 37831, USA

‡ Center for Nanophase Materials Sciences, Oak Ridge National Laboratory, Oak Ridge, TN, 37831, USA

§ Department of Chemistry, University of Tennessee at Knoxville, Knoxville, TN 37916, USA

‖ Present Address: Allegheny College, Meadville, PA, 16355 USA

¶ Present Address: Massachusetts Institute of Technology, Cambridge, MA, 02139 USA

Present Address: East China University of Science and Technology, Shanghai, China 200237

E-mail: abneycw@ornl.gov

Table of Contents

1. General Experimental

Dimethylformamide was purchased from VWR and Dimethylsulfoxide, Methanol, and Sodium Hydroxide were purchased from Sigma-Aldrich. Ammonium Cerium (IV) Hydroxide was purchased from Acros Organics. 2,2'-Bipyridine-5,5'-dicarboxylic Acid (H_2BIPYDC) was purchased from Ark Pharm. Biphenyl-4,4'-dicarboxylic acid (H_2BPDC) and Copper (II) Nitrate Trihydrate were purchased from Sigma-Aldrich. All chemicals listed were used without further purification or modification. Thermogravimetric Analysis (TGA) spectra were recorded on a TA Instruments TGA Q50 using a platinum pan. Powder X-Ray Diffraction Patterns were collected using a PANalytical Empyrean Cu-source diffractometer. Surface Area data were collected via N_2 adsorption isotherms collected under cryogenic conditions on a Micromeretics Tristar; data were analyzed and surface areas determined by application of the BET model. ICP-OES Analysis was performed using a Thermo Fisher iCAP 7400. Samples were diluted using a 2% HNO_3 matrix and analyzed using a 5-point calibration curve over the range of 1 - 25 ppm. Metalated MOFs were digested in H_3PO_4 with 1-2 drops of HF, which was then diluted in the aforementioned HNO_3 matrix. Catalytic experiments were collected using an Altamira Instruments AMI-200 temperature-controlled microreactor with on-line gas chromatograph. The scanning electron microscope (SEM) images were obtained in a Carl Zeiss Merlin SEM operating at 1 kV for imaging with no tilt and 20 kV for the EDX with a 30 tilt. The energy-dispersive x-ray spectroscopy (EDX) results were obtained with a system from Bruker Nano GmbH using a XFlash detector 5030. The sample was tilted toward the detector to help reduce the absorption of the x-rays in the side walls of the rough surface. The Merlin SEM has a "Gemini" column for lower operating voltages so 1 kV was chosen for imaging to help reduce the charging. With the exception of XAFS data discussed below, all fits and data analysis were performed using OriginPro

2015 software. CHN Analysis was performed by Midwest Microlab, Inc, 7212 N. Shadeland Ave, Suite 110, Indianapolis, IN 46250. Samples for CHN analysis were packed into pre-weighed capsules in an inert atmosphere (N_2) glovebox.

2. Characterization

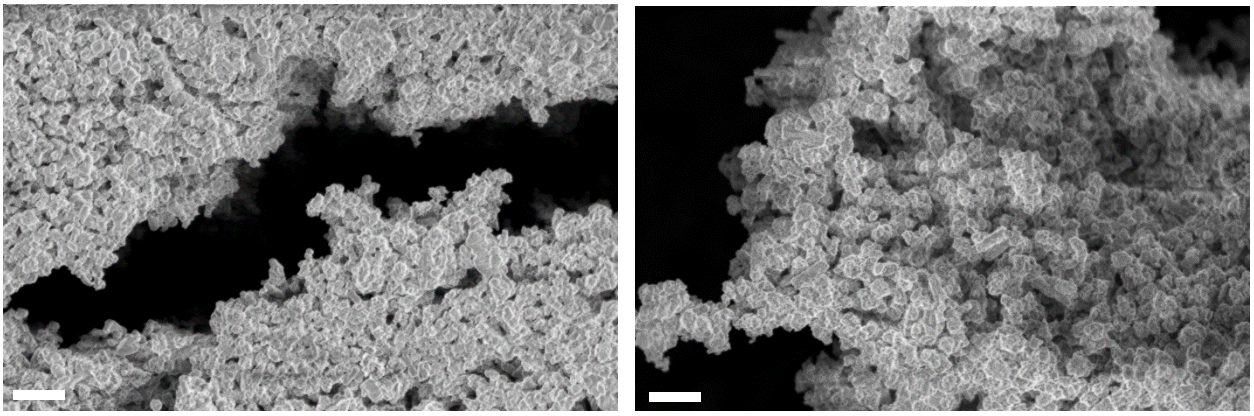

Figure S1. (Left) SEM images of UiO-67(Ce) as reported previously, and (Right) UiO-67-BIPY-50%. Scale bar is 1 μm.

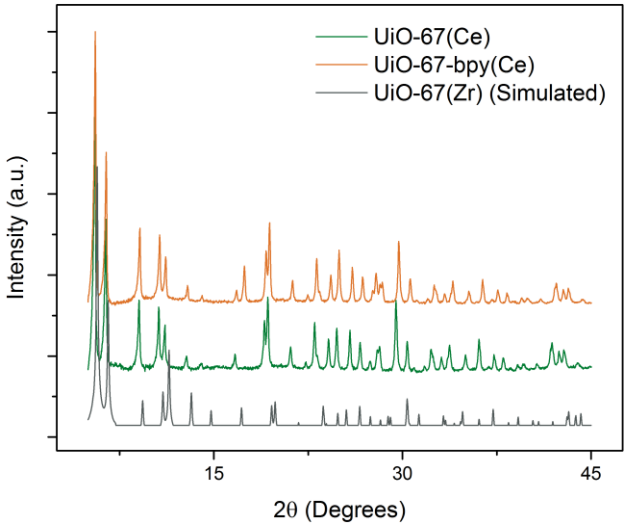

Figure S2. PXRD of UiO-67-BIPY-50% MOF, the previously reported UiO-67(Ce), and a simulated PXRD pattern for the archetypical UiO-67(Zr), demonstrating the successful formation of the UiO-67-bipy MOF. The difference in peak position compared to the simulated UiO-67(Zr) is due to the larger unit cell resulting from use of Ce(IV) in place of Zr(IV).

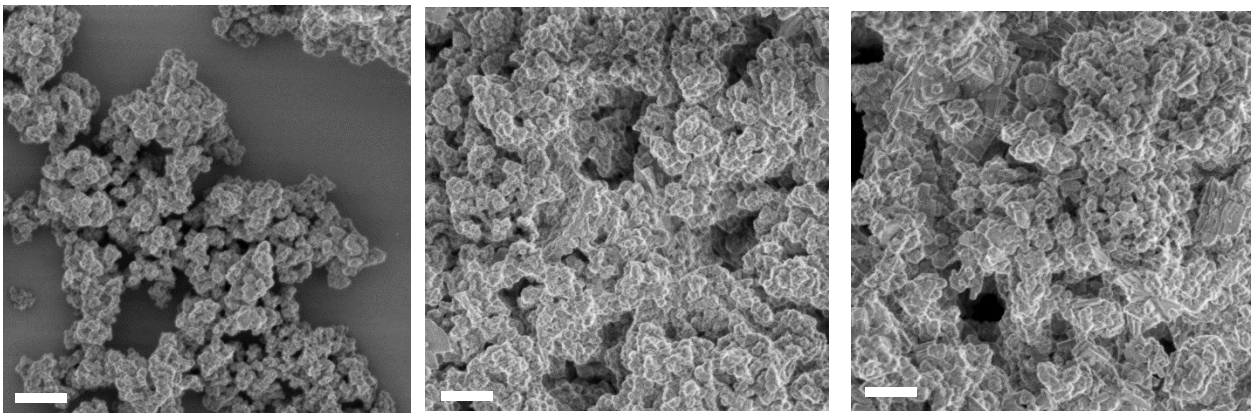

Figure S3. From Left to Right, SEM images of UiO-BIPY-10%, -25% and -50% after loading with $Cu(NO_3)_3$. Scale bar in all images is 1 μm.

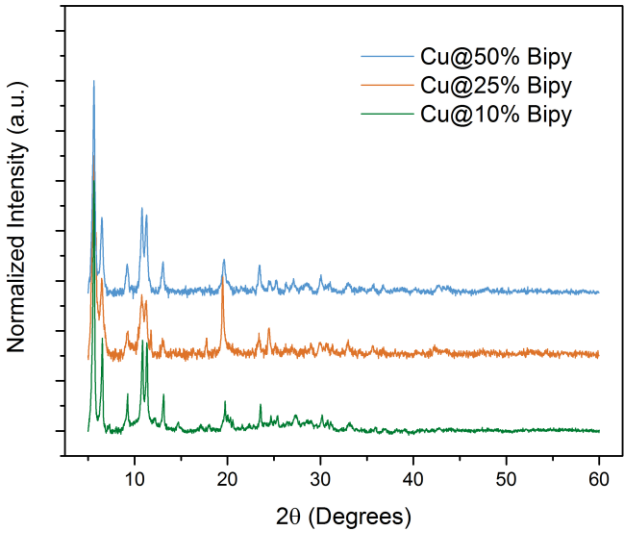

Figure S4. PXRD of UiO-67-BIPY-XX% MOFs after metalation with $Cu(NO_3)_2$. Ordering is retained in all MOF templates, as demonstrated by the presence of diffraction peaks beyond 30°.

Table S1. CHN Analysis for UiO-67-bpy(X%) MOF Templates

	Theoretical			Experimental		
	C	H	N	C	H	N[a.]
UiO-67(Ce)	41.8%	2.2%	0%	40.7%	2.9%	2.5%
-10%	41.2%	2.1%	0.7%	39.9%	2.9%	2.4%
-25%	40.2%	2.0%	1.7%	38.7%	2.8%	4.8%
-50%	38.7%	1.9%	3.5%	36.2%	2.6%	6.6%

a. Experimental N content is elevated due to contributions resulting from preparing analytical samples in an N_2-atmosphere glove box.

Table S2. ICP-OES determined Ce:Cu ratio for Cu-loaded UiO-67-bpy(X%) MOF Templates

Bpy-doping	**Ce:Cu Ratio**
10%	9.6:1
25%	6.2:1
50%	3.2:1

Table S3. Specific surface areas and volumetric surface areas of CuO@CeO_2-XX% MOF-templated materials.

Sample	**Specific Surface Area (BET) (m^2 g^{-1})**	**Specific Surface Area (Langmuir) (m^2 g^{-1})**	**Volumetric Surface Area (m^2 cm^{-3})[a.]**
CuO@CeO_2-10%	77.6	87.7	594
CuO@CeO_2-25%	55.3	76.3	423
CuO@CeO_2-50%	65.5	92.2	501

a. Volumetric surface areas calculated using BET specific surface area.

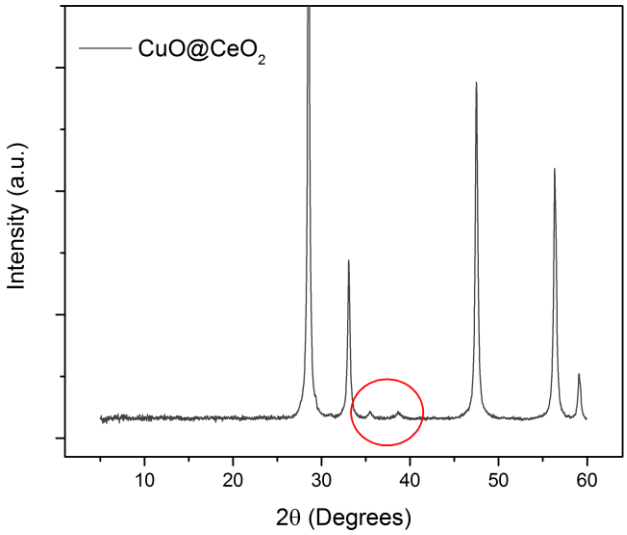

Figure S6. PXRD of 10% CuO mixed with CeO_2; CuO peaks are clearly visible. In contrast, CuO@CeO_2-10% displays no CuO peaks, revealing a chemical difference rather than a limitation in the instrument.

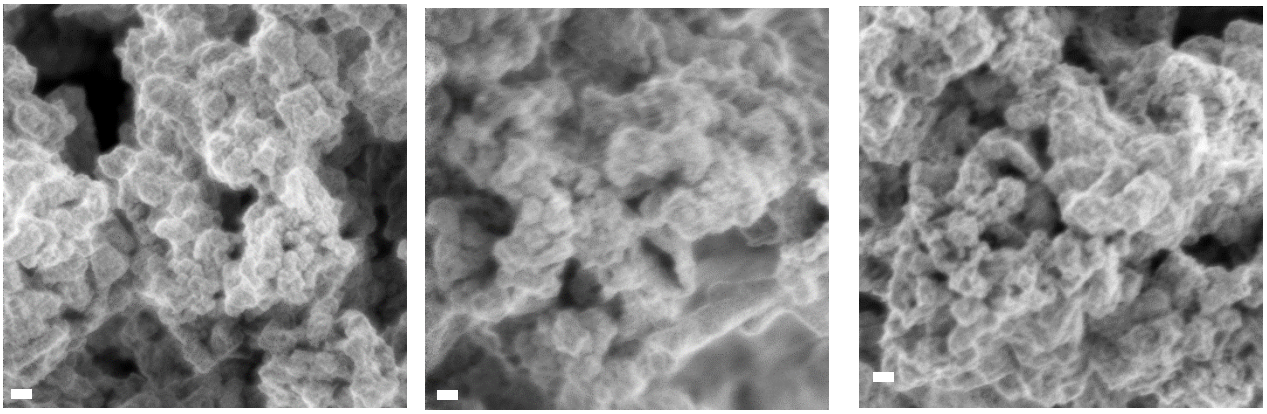

Figure S7. From Left to Right, SEM images of CuO@CeO_2-10%, -25%, and 50%. The scale bar in all images is 100 nm.

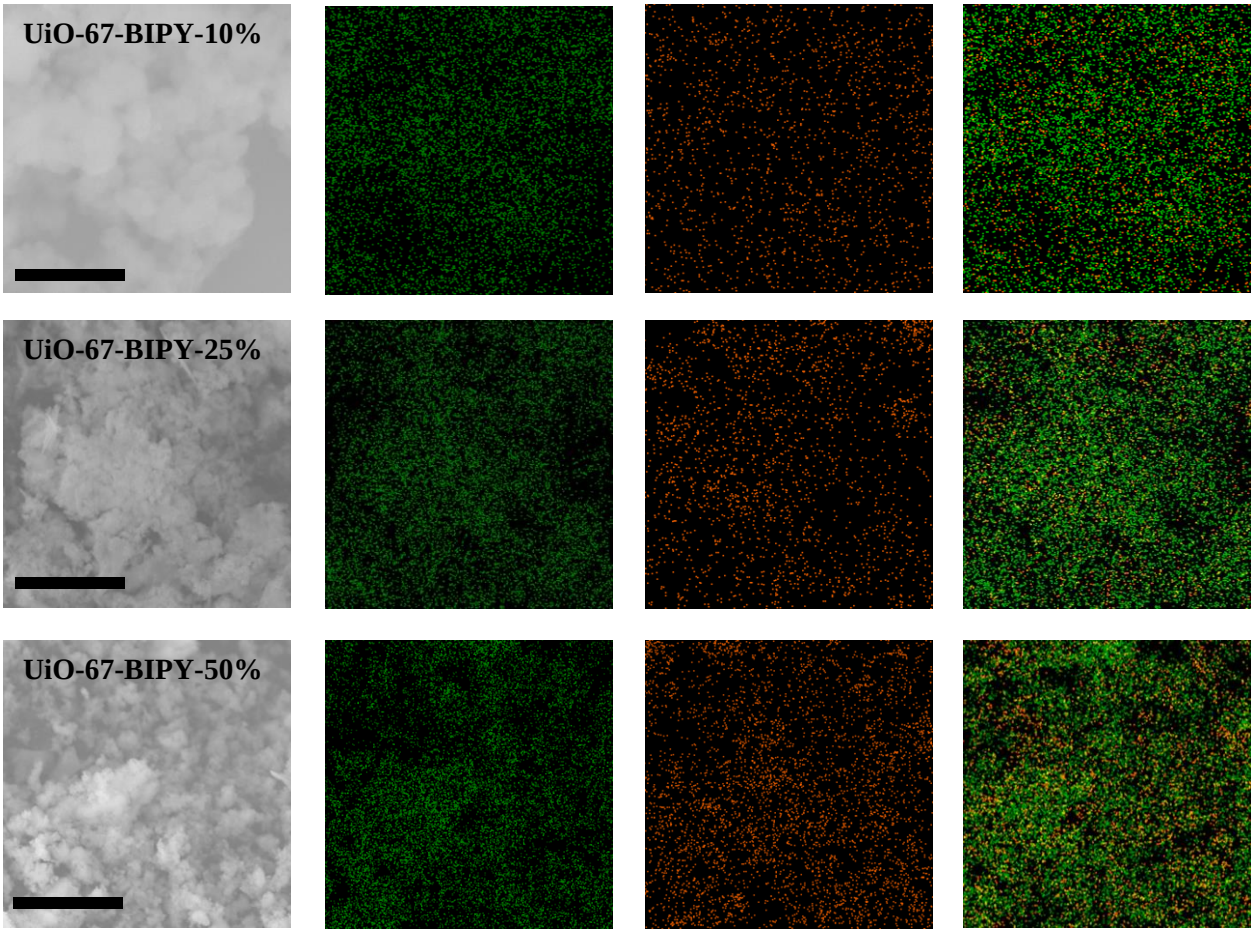

Figure S5. EDX of Cu-loaded UiO-BIPY-XX% MOFs. Ce is displayed in green, Cu is displayed in orange. Columns show the area of analysis, the Ce distribution, the Cu distribution, and the superposition of Ce and Cu. Scale bars are 7 μm.

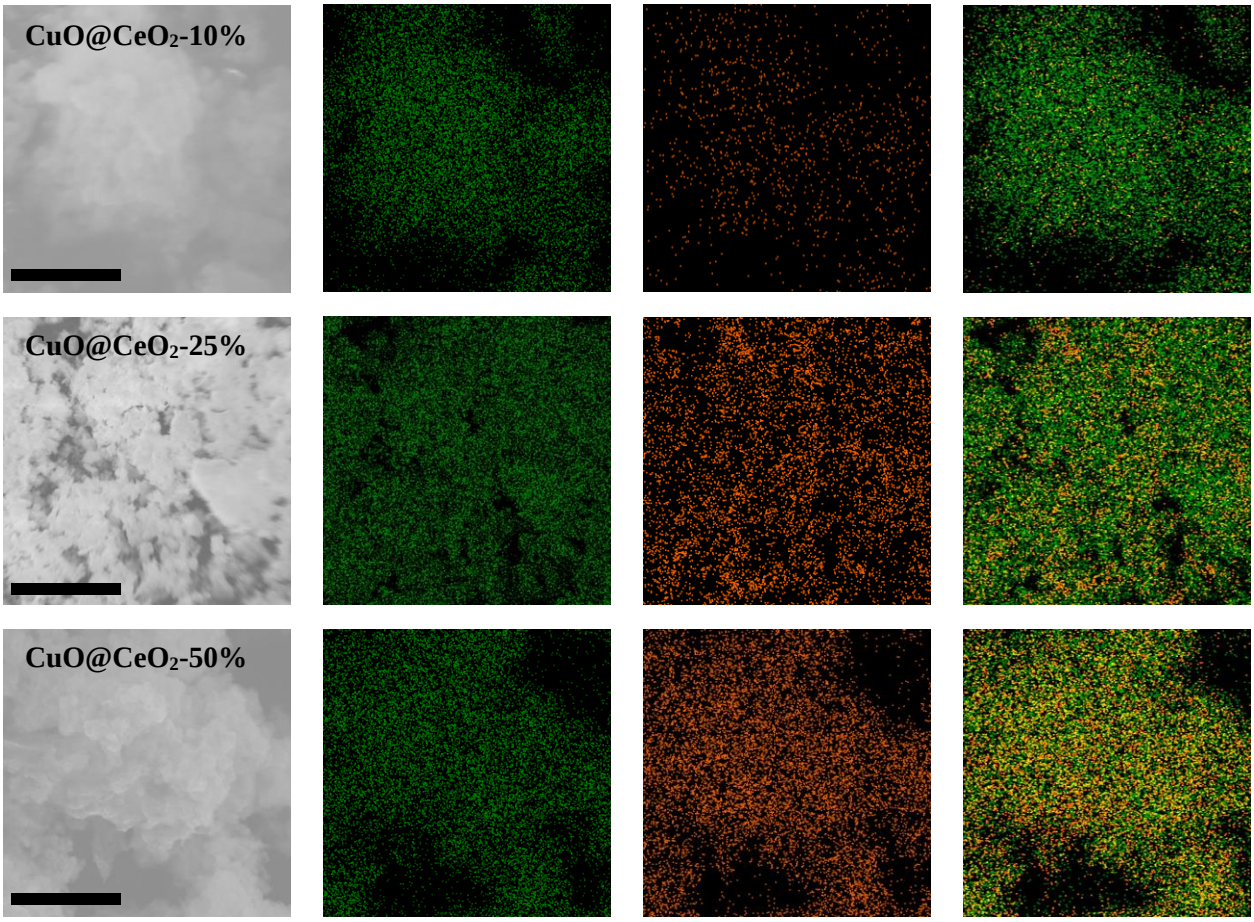

Figure S8. EDX elemental mapping for CuO@CeO_2-XX% systems. Ce is displayed in green, Cu is displayed in orange. Columns show the area of analysis, the Ce distribution, the Cu distribution, and the superposition of Ce and Cu. Scale bars are 7 μm.

3. EXAFS Fitting

CuO@CeO_2-10% The -10% system was fit using only the CuO crystal structure and the Cu-Ce scattering path. Efforts were also attempted to fit the data using scattering paths from the Cu^0 metal, but the resulting fit was inferior both with regards to goodness-of-fit (R-factor) and also statistical considerations (χ_v^2). The model for the final fit included parameters for S_0^2, ΔE_0, 4 ΔR parameters (2 oxygen, 1 copper, and 1 cerium), 2 σ^2 parameters (light scatterers and heavy scatterers), and a variable N_{degen} for the Cu-Ce scattering path (9 variables). Data were fit over the R-range of 1 – 4 Å, and k-range of 3 - 10.4 $Å^{-1}$ (13.9 independent points). Only single scattering paths were used to fit the data. The refined parameters are summarized in Table S3; final structural details are provided in Table S4.

CuO@CeO_2-25% and -50% The -25% and -50% systems were fit using the same structure model, which contained scattering paths from only CuO and Cu^0 metal. Due to the formation of the nanoparticles as determined by microscopy and PXRD, interfacial contributions were calculated to contribute less than 10% to the spectrum and thus are not resolvable by EXAFS. The final fit included parameters for ΔE_0, the fraction of CuO and Cu^0, 3 ΔR parameters (2 oxygen, 1 copper from CuO), 3 σ^2 parameters (CuO light scatterers, CuO heavy scatterers, Cu^0 scatterers), and an isotropic scaling factor (α) for the face-centered cubic Cu^0 metal (9 parameters). Assuming interatomic distances in Cu^0 domains change isotropically due to possessing a cubic spacegroup, multiplication of R_{eff} for the Cu^0 metal scattering paths by α affords a statistically rigorous way to replace multiple ΔR parameters that would otherwise be required. The fractional contribution of Cu^0 was defined as 1-$frac_{(CuO)}$, where $frac_{(CuO)}$ was the fitted parameter for the fractional contribution of CuO to the structure model. Data were fit over the same range as CuO@CeO_2-10%, affording 13.9 independent points. Only single scattering paths were used to fit the data. As

S_0^2 and degeneracy are directly correlated, S_0^2 was initially fixed at 1, affording good fits of the data. Attempts to remove this restraint resulted in refined values which were physically unreasonable (>> 1) and degradation of the fit. S_0^2 was thus set equal to 1 for fits of the -25% and -50% data. The refined parameters are summarized in Table S3; final structural details are provided in Table S4.

Table S4. Refined Parameters for EXAFS Fits of CuO@CeO_2-XX% Materials.

Parameter	**CuO@CeO_2-10%**	**CuO@CeO_2-25%**	**CuO@CeO_2-50%**
S_0^2	0.69 ± 0.03	---	---
ΔE_0 (eV)	-1.8 ± 0.9	0.0 ± 0.8	0 ± 1
CN_{Ce}	2.4 ± 0.9	---	---
$Frac_{(Cu\text{-}0)}$ (%)	---	75 ± 6	75 ± 7
ΔR_{O1} (Å)	-0.017 ± 0.007	-0.014 ± 0.006	-0.009 ± 0.009
ΔR_{O2} (Å)	-0.01 ± 0.03	0.06 ± 0.04	0.08 ± 0.07
ΔR_{Cu} (Å)	0.13 ± 0.03	0.02 ± 0.03	0.02 ± 0.03
ΔR_{Ce} (Å)	0.05 ± 0.03	---	---
α	---	0.08 ± 0.02	0.23 ± 0.04
$\sigma^2_{(Light)}$ ($\times 10^{-3}$ Å^2)	3.0 ± 0.1	2.5 ± 0.8	3 ± 1
$\sigma^2_{(Heavy)}$ ($\times 10^{-3}$ Å^2)	11 ± 2	22 ± 8	18 ± 9
$\sigma^2_{(Cu\text{-}0)}$ ($\times 10^{-3}$ Å^2)	---	12 ± 4	7 ± 3
R-factor	0.7%	0.5%	0.9%

Table S5. Average Interatomic Distances and Degeneracies Determined by EXAFS Fits for CuO@CeO_2-XX% Materials.

	CuO@CeO_2-10%		**CuO@CeO_2-25%**		**CuO@CeO_2-50%**	
Path	*Degen.*	*Dist. (Å)*	*Degen.*	*Dist. (Å)*	*Degen.*	*Dist. (Å)*
Cu-O_1	4	1.94	3 ± 0.3	1.94	3 ± 0.3	1.95
Cu-O_2	2	2.77	1.5 ± 0.1	2.84	1.5 ± 0.1	2.86
Cu-Cu_1	4	3.02	3 ± 0.3	2.92	3 ± 0.3	2.92
Cu-Cu_2	4	3.21	3 ± 0.3	3.10	3 ± 0.3	3.10
Cu-Ce	2.4 ± 0.9	3.63	---	---	---	---
Cu-Cu^0_1	---	---	4 ± 0.8	2.75	4 ± 0.8	2.79
Cu-Cu^0_2	---	---	1.5 ± 0.3	3.90	1.5 ± 0.3	3.85